Journal of Materials Chemistry A

ROYAL SOCIETY OF CHEMISTRY

PAPER

View Article Online
View Journal

Cite this: DOI: 10.1039/d1ta00363a

A rigorous electrochemical ammonia electrolysis protocol with *in operando* quantitative analysis†

Yejin Yang,‡[a] Jeongwon Kim,‡[a] Hyoi Jo,[a] Arim Seong,[a] Minzae Lee,[b] Hyung-Ki Min,[b] Myung-gi Seo,[b] Youngheon Choi[b] and Guntae Kim *[a]

Ammonia has emerged as an attractive liquid fuel for hydrogen production owing to its facile transportation, high capacity of hydrogen storage, and ecofriendly environmental products (N_2 and H_2). Moreover, the electrolysis of ammonia to produce nitrogen and hydrogen only requires an external voltage of 0.06 V theoretically, which is much lower than the energy needed for water electrolysis (1.23 V). In this study, we propose a well-established procedure using *in operando* gas chromatography that enables us to reliably compare and evaluate the new catalyst for ammonia oxidation. With the protocol, we could distinguish in detail the competitive oxidation reaction between the ammonia oxidation and oxygen evolution reactions with real-time monitoring. Using a flower-like electrodeposited Pt catalyst, we have efficiently produced hydrogen with less power consumption of 734 L_{H_2} kW h^{-1}, which is significantly lower than that of the water-splitting process (242 L_{H_2} kW h^{-1}). The use of this rigorous protocol should help to evaluate the practical performances for ammonia oxidation, thus enabling the field to focus on viable pathways towards the practical electrochemical oxidation of ammonia to hydrogen.

Received 14th January 2021
Accepted 26th March 2021

DOI: 10.1039/d1ta00363a

rsc.li/materials-a

Introduction

Owing to the high capacity of hydrogen storage and environmental friendliness, the ammonia (NH_3) electro-oxidation reaction has received increasing interest as an advanced technology to produce hydrogen using less thermodynamic energy than water electrolysis.[1–4] Theoretically, the electrolysis of ammonia to produce nitrogen and hydrogen only requires an external voltage of 0.06 V, which is much lower than the energy needed for water electrolysis (1.23 V), leading to high theoretical energy efficiency.[5–7] According to Vitse *et al.*, ammonia electrolysis consumes 95% less energy than water electrolysis during producing hydrogen under mild conditions.[3] Also in terms of energy density, the ammonia has a volumetric energy density of 15.6 MJ L^{-1} which is 70% higher than that of liquid hydrogen (9.1 MJ L^{-1}). Moreover, ammonia is easily condensed at ambient temperature (under a pressure of 8 bar), making it suitable for transportation and storage. Consequently, the use of ammonia as a carbon-free hydrogen carrier has several advantages to succeed in widespread applications.

Ideally, the decomposition of ammonia is an attractive application for hydrogen production and comprises the reversal of the Haber–Bosch process.[4,8,9] In the liquid ammonia decomposition system, H_2O is reduced at the cathode to H_2 (eqn (1)) while NH_3 is oxidized at the anode to N_2 (eqn (2)), generating the gas phase of hydrogen and nitrogen from an ammonia solution (eqn (3)).

$$\text{Cathodic reaction: } 6H_2O + 6e^- \rightarrow 3H_2(g) + 6OH^- \quad (1)$$

$$\text{Anodic reaction: } 2NH_3(aq) + 6OH^- \rightarrow N_2(g) + 6H_2O + 6e^- \quad (2)$$

$$\text{Total reaction: } 2NH_3(aq) \rightarrow N_2(g) + 3H_2(g) \quad (3)$$

$$\text{Competitive anodic reaction: } 6OH^- \rightarrow 3/2O_2 + 6H_2O + 6e^- \quad (4)$$

In the liquid ammonia decomposition process, it is well known that the anodic reaction of ammonia oxidation reaction (eqn (2)) competes with the side reaction of oxygen evolution reaction (eqn (4)).

Herein, through *in operando* analysis, we aim to track the real-time gas products and compare the consumption of power per hydrogen produced for the ammonia electrolysis with water-splitting during electrochemical measurements. Following this analysis, firstly the ammonia decomposition products can be successfully identified as H_2 and N_2 when using the most promising Pt electro-deposited electrode for this reaction in aqueous media. The well-controlled Pt electrode exhibited an exceptionally high electrochemical performance (50 mA cm^{-2} over 10 hours) in practical application. Moreover, we determine accurately the actual amount of H_2 and N_2 (or O_2) and calculate the faradaic efficiency during operation. Besides, the higher

[a]*Department of Energy Engineering, Ulsan National Institute of Science and Technology (UNIST), Ulsan 44919, Republic of Korea. E-mail: gtkim@unist.ac.kr; Fax: +82-52-217-2909; Tel: +82-52-217-2917*

[b]*Lotte Chemical R&D Center, Daejeon 34110, Republic of Korea*

† Electronic supplementary information (ESI) available. See DOI: 10.1039/d1ta00363a

‡ These authors contributed equally to this work.

hydrogen production per power than water splitting provides definite evidence for an efficient hydrogen production electrochemical system. However, the above discussion also disproves that the mechanism of the ammonia oxidation reaction (AOR) conducted on Pt electrodes is rather complicated. Therefore, we also suggested a standardized protocol towards the electrochemical tendency of the AOR according to the electrode synthesis process utilizing electrochemical experiments, so that the experimental results can be inferred based on the standard catalyst. The use of this viable protocol will enable more effective analysis of electrochemical systems that focus on the practical application of ammonia electrolysis.

Results and discussion

As shown in Fig. 1, two types of electrodeposited Pt electrode were fabricated with different electrochemical processes (chronopotentiometric deposition *vs.* cyclic voltammetric deposition). The Pt particles were homogeneously deposited on the nickel substrate *via* both processes, but with different morphologies. The crystalline structure and morphology of each electrode are presented in Fig. 2. In Fig. 2a, the crystal structure profiles were analyzed by X-ray diffraction (XRD) measurements. On the nickel substrate, the XRD patterns featured three small polycrystalline Pt peaks as Pt(111), Pt(200), and Pt(220) at 40°, 46°, and 68°, respectively.[10–13] In the Pt electrode prepared *via* the cyclic voltammetric (CV) deposition process, the crystallinity of Pt improved in both Pt(111) and Pt(200) as the number of cycles was increased. With the Pt(111) and Pt(200), the average crystalline size of Pt was also investigated using the Debye–Scherrer equation (Table S1†).[14–16] The average crystalline size of Pt obtained *via* the CV process was about 10 nm (diameter) independent of the number of CV cycles, which is smaller than that of the Pt electrode synthesized by the chronopotentiometry (CP) deposition process (diameter of ~20 nm). In Fig. 2b–f, SEM profiles show the morphology of Pt on the nickel substrate for CP and CV electrodes. Under chronopotentiometric deposition of Pt, agglomerated round shape dense particles with a rough surface were obtained (Fig. 2b). Meanwhile, the size of Pt particles synthesized *via* the CV method in 100, 200, 400, and 500 cycles was smaller than that obtained *via* the CP method, which matches well with the trend of particle size calculated from XRD.[5] Interestingly, the 400 cycle electrode showed a flower-like platinum structure on a nickel substrate, which might be attributed to the enhanced electrochemical performance with highly catalytically active sites. Compared to CP synthesis, CV acts as an alternating redox process during the cycling process, which involves both deposition and dissolution of Pt. The continuous redox reactions (cathodic/anodic scans) are involved in nucleation and growth of Pt particles/atoms on a nickel substrate.[17] During the reductive scan, hydrogen (H_2) is generated on the nickel substrate following possible reactions.[18,19]

$$PtCl_6^{2-} + 2e^- \rightarrow PtCl_4^{2-} + 2Cl^- \quad (5)$$

$$PtCl_4^{2-} + 2e^- \rightarrow Pt + 4Cl^- \quad (6)$$

$$Pt + 2H^+ \rightarrow Pt(H_2)_{ads} \quad (7)$$

And then, during the oxidative scan, further electrochemical reactions proceeded.

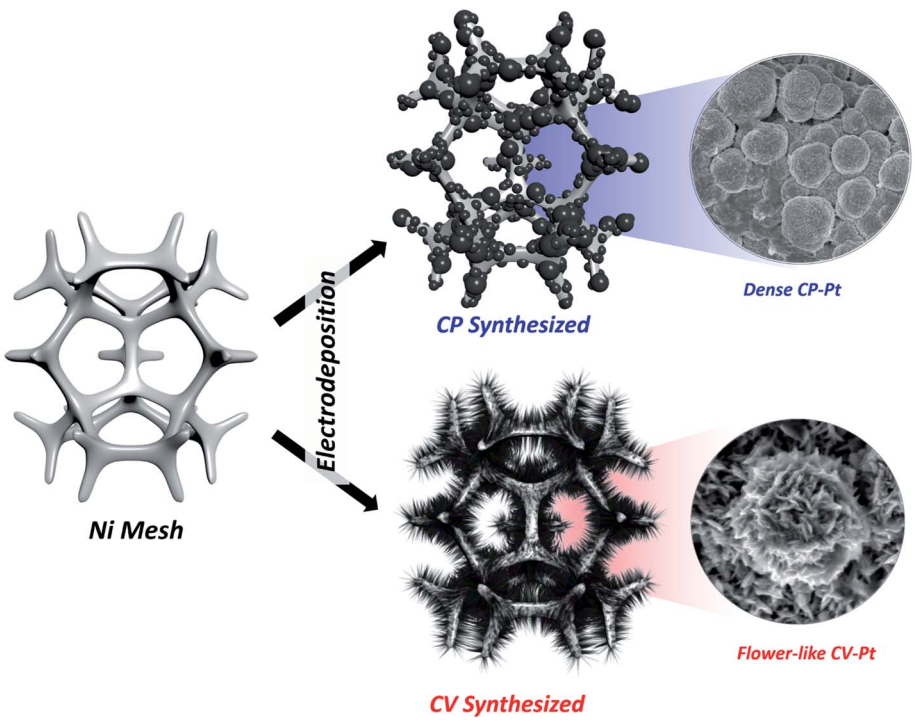

Fig. 1 Schematic illustration of the CP-Pt and CV-Pt electrodes.

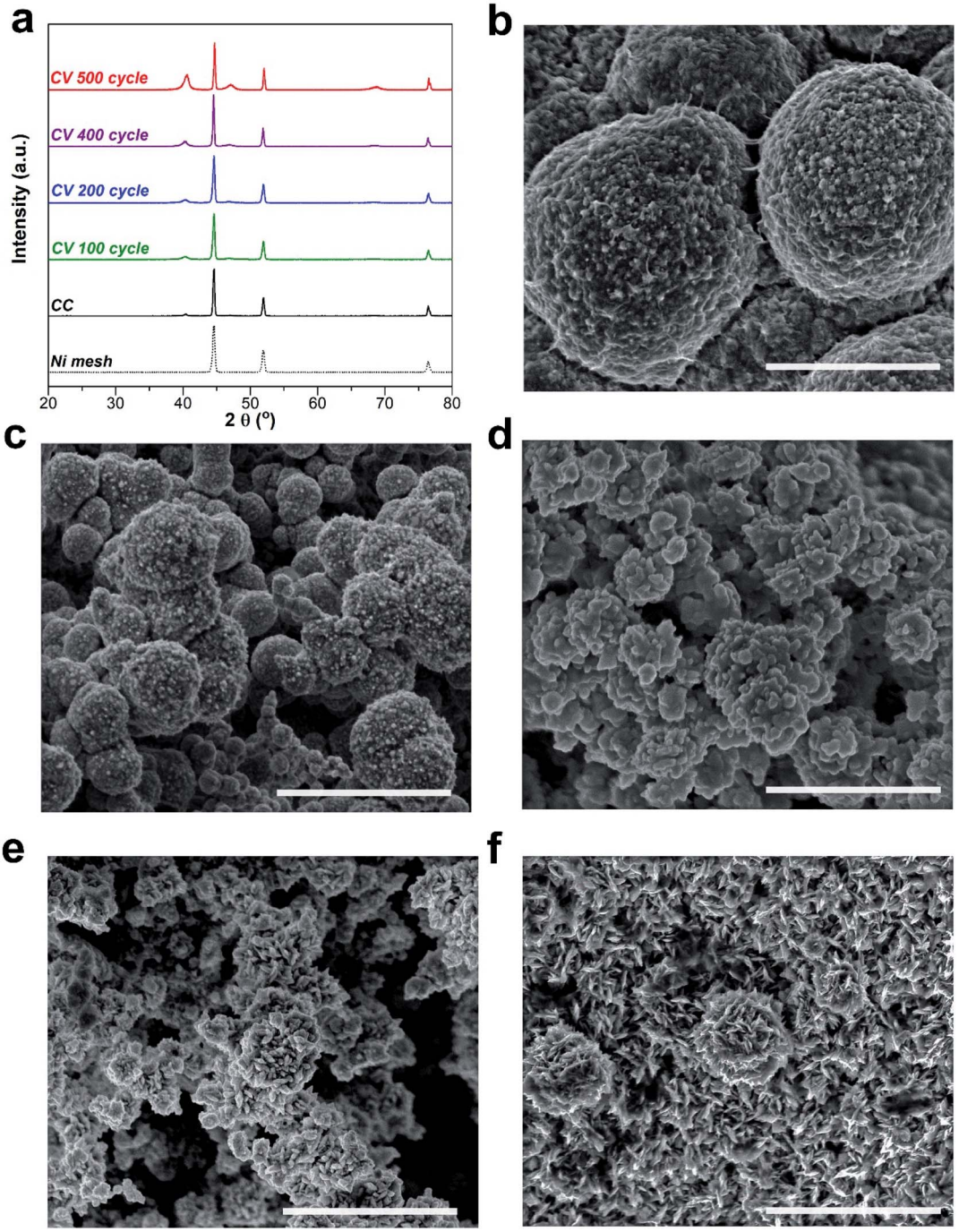

Fig. 2 (a) XRD patterns of six samples including bare Ni mesh, and Pt-deposited Ni mesh prepared by different electrochemical processes. SEM images of electrodeposited Pt on Ni mesh (b) by the CP process and at various cycle numbers: (c) 100, (d) 200, (e) 400 and (f) 500 cycles. Scale bar: 1 μm.

$$Pt(H_2)_{ads} + H_2O \rightarrow Pt(O)_{ads} + H_2(g) + 2H^+ + 2e^- \quad (8)$$

$$Pt(O)_{ads} + H_2O \rightarrow PtO_2 + 2H^+ + 2e^- \quad (9)$$

After that, during the again-reductive scan in cyclic voltammetry, reactions (10)–(12) proceed at a low overpotential window, leading to deposition of nanoparticles/atoms of Pt metal on the substrate.

$$Pt(O)_{ad} + 2H^+ + 2e^- \rightarrow Pt + H_2O \quad (10)$$

$$PtO_2 + 4H^+ + 2e^- \rightarrow Pt^{2+} + H_2O \quad (11)$$

$$Pt^{2+} + 2e^- \rightarrow Pt\ metal \quad (12)$$

As indicated by reaction (8), the desorption of H_2 takes place by the reaction with H_2O, which might be attributed to the

flower-like morphology of Pt as shown in the SEM results. Dendrite growth of Pt metal near the surface is favored due to direct generation of hydrogen bubbles at the substrate, with affects the local hydro-dynamic conditions and flower-like morphology of Pt. With the help of bright-field (BF) STEM, the totally different morphologies of CP-Pt and 500 CV-Pt are confirmed (Fig. S1†). Moreover, TEM-EDS can be performed to confirm that the flower-like morphology belongs to Pt.

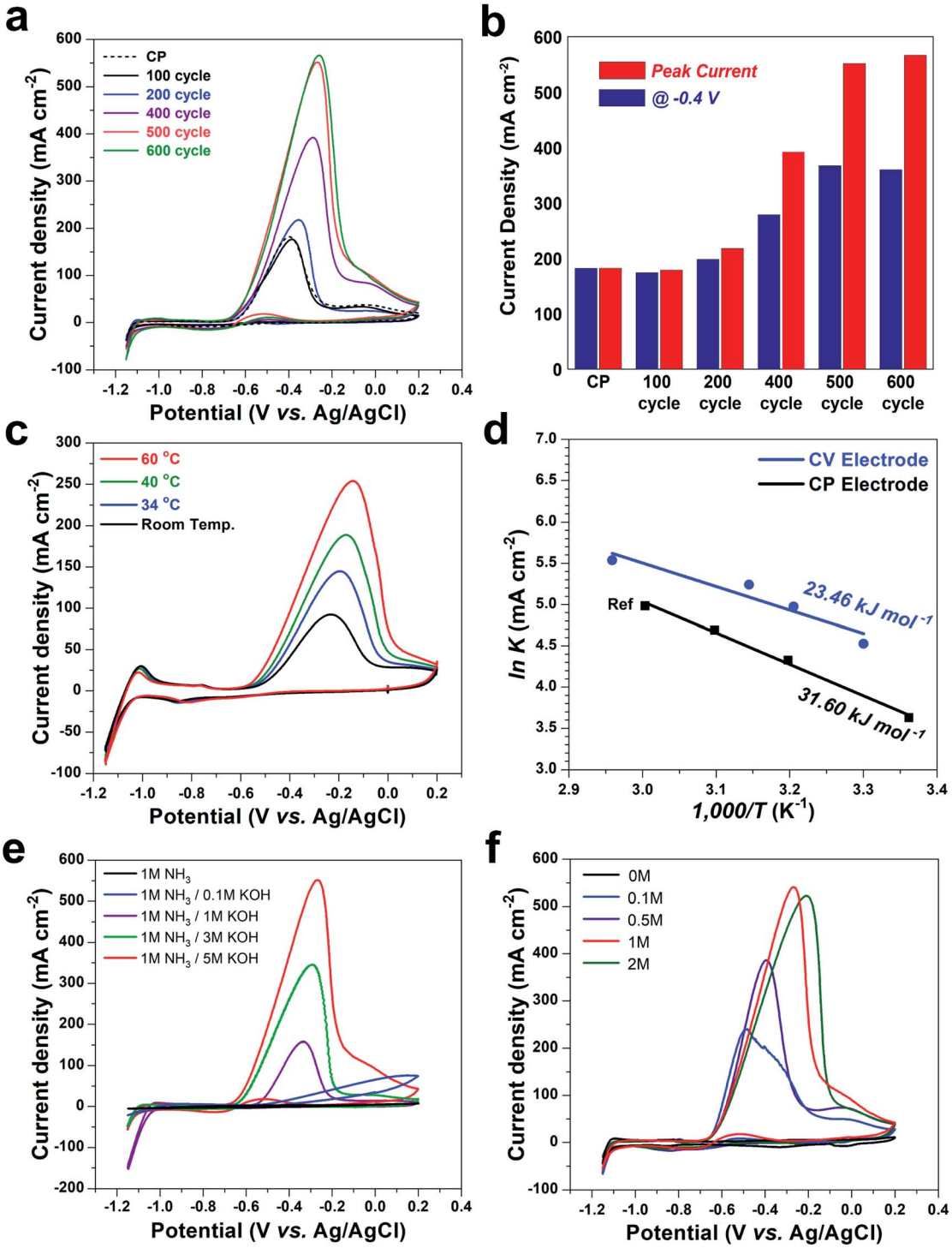

Fig. 3 (a) CVs measured on the CV-Pt electrocatalysts in 5 M KOH/1 M ammonia solution. (b) Comparison of peak current density for different electrodeposition processes. (c) CVs of the 500 CV-Pt on carbon paper at various temperatures from 25 °C to 60 °C. (d) Arrhenius plot. The double-layer capacitance (C_{dl}) of the reference electrode is 4.86 mF cm^{-2}. (e) CVs of the 500 CV-Pt electrode at various KOH concentrations from 0 M to 5 M. (f) CVs of the 500 CV-Pt electrode at various ammonia concentrations from 0 M to 2 M. All CV measurements are recorded at a scan rate 20 mV s^{-1}.

To deeply evaluate the electrocatalytic activity for the ammonia oxidation reaction (AOR), the CP-Pt electrode and CV-Pt electrodes with the different number of CV cycles were evaluated using cyclic voltammograms (CVs) in alkaline media (Fig. 3a). From the CV measurements, the CP-Pt electrode and 100 CV-Pt electrode showed similar peak current densities of 182 and 176 mA cm^{-2}, respectively. In addition, with the increased number of CV cycles, the peak current density is significantly increased and saturated by 500 cycles. After 500 cycles, as the surface grows and the structures become larger with increased surface area, the hydrodynamic stirring by the evolving H_2 is less pronounced, and the diffusion limited growth of Pt to dendritic structures is no longer favored. When this occurs, compact Pt on the flower-like Pt was deposited which might lead to saturated electrochemical performance of the CV electrode. The ammonia oxidation kinetics were also increased for the 500 CV-Pt electrode as shown in Fig. 3b. As shown in Fig. S2,† the AOR mass activity for the 500 CV-Pt electrode was optimized as 4.37 A mg^{-1}, which is higher than that of commercial Pt/C. In addition, the 500 CV-Pt electrode's normalized electrochemical performance with electrochemical surface area (ECSA) was also confirmed (Fig. S3 and S4†). Therefore, the CV deposition process was optimized for the 500 CV-Pt electrode according to the ammonia oxidation performance regarding peak current density and kinetics for the AOR. In the analysis protocol for identifying a promising electrocatalyst for the AOR, the intrinsic catalytic activity for the AOR needs to be investigated with the different AOR activities under various temperature conditions. In Fig. 3c, CV measurements were conducted using 500 CV-Pt on carbon paper to eliminate the activity of the nickel substrate at various temperatures in alkaline media. As the temperature increased, the peak current density for the AOR also increased. With the CV results, we can obtain the apparent activation energy (E_a) calculated using the Arrhenius equation as follows.[20–22]

$$k = Ae^{(-E_a/RT)}$$

where k, A, R, and T represent the reaction rate constant, frequency factor, gas constant, and temperature, respectively. Between the logarithm of current density and the reciprocal of the temperature, the linear increase of current density was confirmed with increased temperatures (Fig. 3d). From the plotted data of the 500 CV-Pt electrode, activation energy (E_a) for ammonia electro-oxidation was calculated to be 21.26 kJ mol^{-1}, indicating that it is a more favorable electrocatalyst for the AOR than the previous Pt-based electrode (31.60 kJ mol^{-1}).[2] The detailed activation energy calculation is shown in the ESI.† It is also worth noting that the activation energy for ammonia electro-oxidation is much lower than that for thermal decomposition (*ca.* 70–170 kJ mol^{-1}).[23,24] From the calculation of E_a for the AOR, we could find the efficient electrocatalyst for the AOR or evaluate the ammonia oxidation or decomposition energy in various processes.

To investigate the catalytic activities of the synthesized catalyst in detail, the effects of not only OH^- ion concentration, but also ammonia concentration should be evaluated. In Fig. 3e, the investigation for the AOR was conducted at various concentrations of KOH because the KOH electrolyte was utilized as a supporting solution for both half-cell and full-cell measurements. From without KOH conditions to 5 M KOH, the overpotentials for the AOR were significantly reduced and the peak current densities were greatly increased. According to the above results, ammonia is easily oxidized to N_2 on a Pt surface at a high concentration of KOH, which might be attributed to the facile absorption of OH^- ions at high concentration of KOH electrolyte. In addition to OH^- ion concentration dependence, the effects of ammonia concentration in the electrolyte were also investigated. Fig. 3f shows the CV measurements with the concentration of ammonia ranging from 0 M to 2 M in 5 M KOH electrolyte. As expected, at the concentration of ammonia of 0 M, there is no ammonia oxidation peak. From the 0.1 M to 1 M concentration, the ammonia oxidation peak current was gradually increased. At 2 M concentration of ammonia, however, the peak current for ammonia oxidation was slightly decreased. The decreased peak current density at 2 M ammonia electrolyte might be attributed to metal oxidation reaction forming metal oxynitrides that hinder the ammonia oxidation reaction.[25] Therefore, from the above electrochemical analysis, we have optimized the specific conditions for the 500 CV-Pt electrode for the AOR as 1 M NH_3(aq) in 5 M KOH solution at 60 °C. The ammonia electrolysis in single-cell and half-cell tests was performed under the optimized conditions.

For practical application of ammonia oxidation and hydrogen production, we have investigated the single-cell electrochemical performance for both the hydrogen evolution reaction (HER) and ammonia oxidation reaction (AOR) in Fig. 4. The CV-Pt electrodes with various cycles were used as the anode (ammonia oxidation electrode), and Pt wire was used as a cathode for the hydrogen evolution electrode. The single-cell measurements were conducted in a three-electrode configuration using a Ag/AgCl reference electrode to clearly distinguish each electrochemical reaction.[15,16,26] Stability tests of the anodes synthesized with various number of cycles ranging from 100 to 500 were conducted (Fig. 4a). Among the electrocatalysts, the 500 CV-Pt electrode exhibits an excellent durability performance for 10 h at a current density of 50 mA cm^{-2}. In Fig. 4a, all of the stability profiles show a potential range from 0.6 to 0.7 V in the beginning and then a sharp jump to above 1.5 V as time passes. The sharp rise in cell potential occurs after a long time when the number of CV cycles is higher. From the three-electrode configuration, it is determined that the sharp rise in cell potential was caused by the changed anodic reaction. These phenomena could be explained by competition between eqn (2) and (4) for the oxidation of NH_3(aq) and the oxidation of OH^-, respectively. At the beginning of electrolysis, sufficient ammonia is adsorbed on the catalyst surface for ammonia oxidation. As electrolysis proceeds, however, a continuously degraded and sharply raised cell voltage is detected, which is attributed to consumed ammonia sources and the poisoning effect of the Pt surface during ammonia oxidation.[3,6] For the detailed evaluation for practical application, the durability performance and *I–V* curve profile should be investigated as

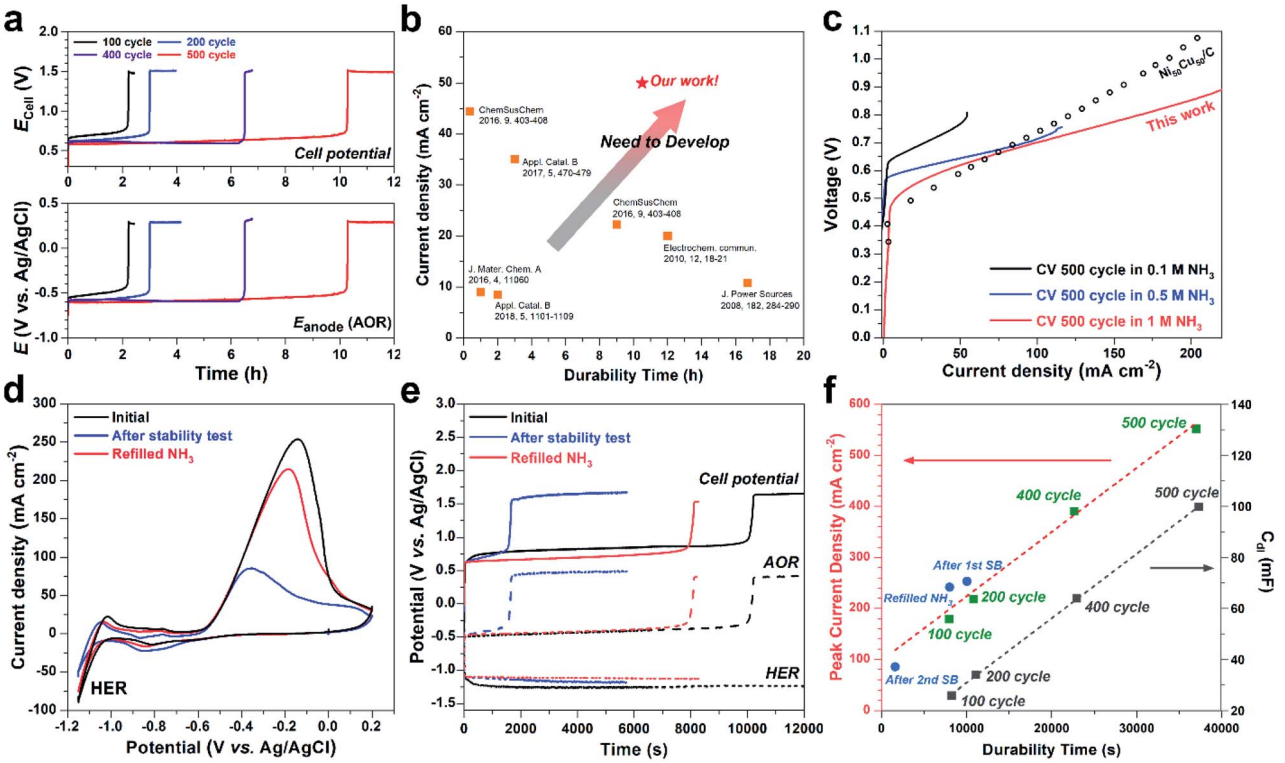

Fig. 4 (a) Stability test of the CV-Pt electrodes at 60 °C at a constant current density of 50 mA cm^{-2} using 5 M KOH containing 1 M ammonia. (b) Maximum durability time and operating current density for the present work with that of previous studies for the electro-oxidation of ammonia. (c) Polarization *I*–*V* profiles of 500 CV-Pt at various ammonia concentrations. (d and e) Relationship between peak current density in CVs and durability time. (f) Linear-tendency of durability time with ECSA and peak current density.

shown in Fig. 4b and c. The stability performance at a high current density region (50 mA cm^{-2}) was evaluated over 10 hours, revealing excellent electrochemical durability compared to that of recently reported AOR electrocatalysts.[1,2,4,6,27–29] The stability performance and maximum durability time of the 500 CV-Pt electrode at room temperature were also confirmed in Fig. S5.† In Fig. 4c, *I*–*V* profiles present the electrochemical performance corresponding to different current density regions of each electrocatalyst. Because the electrochemical properties for different current density conditions need to be investigated for application under various operating conditions, the comparison has been made in both the high and low current ranges. The 500 CV-Pt electrode showed low overpotential for ammonia oxidation (10 mA cm^{-2} at 0.51 V) as well as excellent ammonia oxidation performance at a high current density region (200 mA cm^{-2} at 0.85 V). From the detailed results in Fig. 4b and c, the most suitable electrocatalyst for practical application could be determined.

The relationship between peak current density in CV tests and stability in the application is illustrated in Fig. 4d–f. The electrical stability of the electrode showed a similar trend to peak current density. After the stability test using the 'initial electrode', the peak current density of the electrode was dramatically decreased (denoted as after stability test with blue color). Corresponding to decreased peak current density, the electrode has poor stability performance in Fig. 4e. However, after refilling the NH_3(aq) source in an electrolyte, both peak current density and stability performance were increased. Interestingly, the stability performance in the practical application linearly increases with peak current density in CV tests (Fig. 4f). Furthermore, the stability performance also has a linear tendency with electrochemical surface area (ECSA) of the catalyst (Fig. S3†).[30,31] With these results, we concluded that the stability performance of electrocatalyst is attributed to the reduced ammonia source in electrolyte as well as initial physical or electrochemical surface area, which could be treated as a capacity for preventing the poisoning effect. Also, it is worth noting that we could roughly predict the stability performance from the CV profiles.

To determine the composition of gas products in practical applications, *in operando* quantitative gas chromatography (GC) measurement was conducted. Before the ammonia electrolysis with GC analysis, we have cleaned the impurity from residue gas in the system for quantitative analysis of each gas (Fig. S6†). The cleaning and preparation procedures for *in operando* GC analysis are described in detail in the Experimental section and ESI Note 2† with the *in operando* GC test protocol with an example. As shown in Fig. 5a, a systematic experiment was conducted by connecting a closed liquid ammonia decomposition device (AOR + HER) directly to a GC instrument. With the three-electrode system, firstly, we have investigated the Faraday efficiency (FE) of hydrogen production at each specific potential (Fig. 5b). In the potential window from −0.25 V to 0.35 V *vs.* Ag/AgCl, the Faraday efficiency of the 500 CV-Pt electrode was

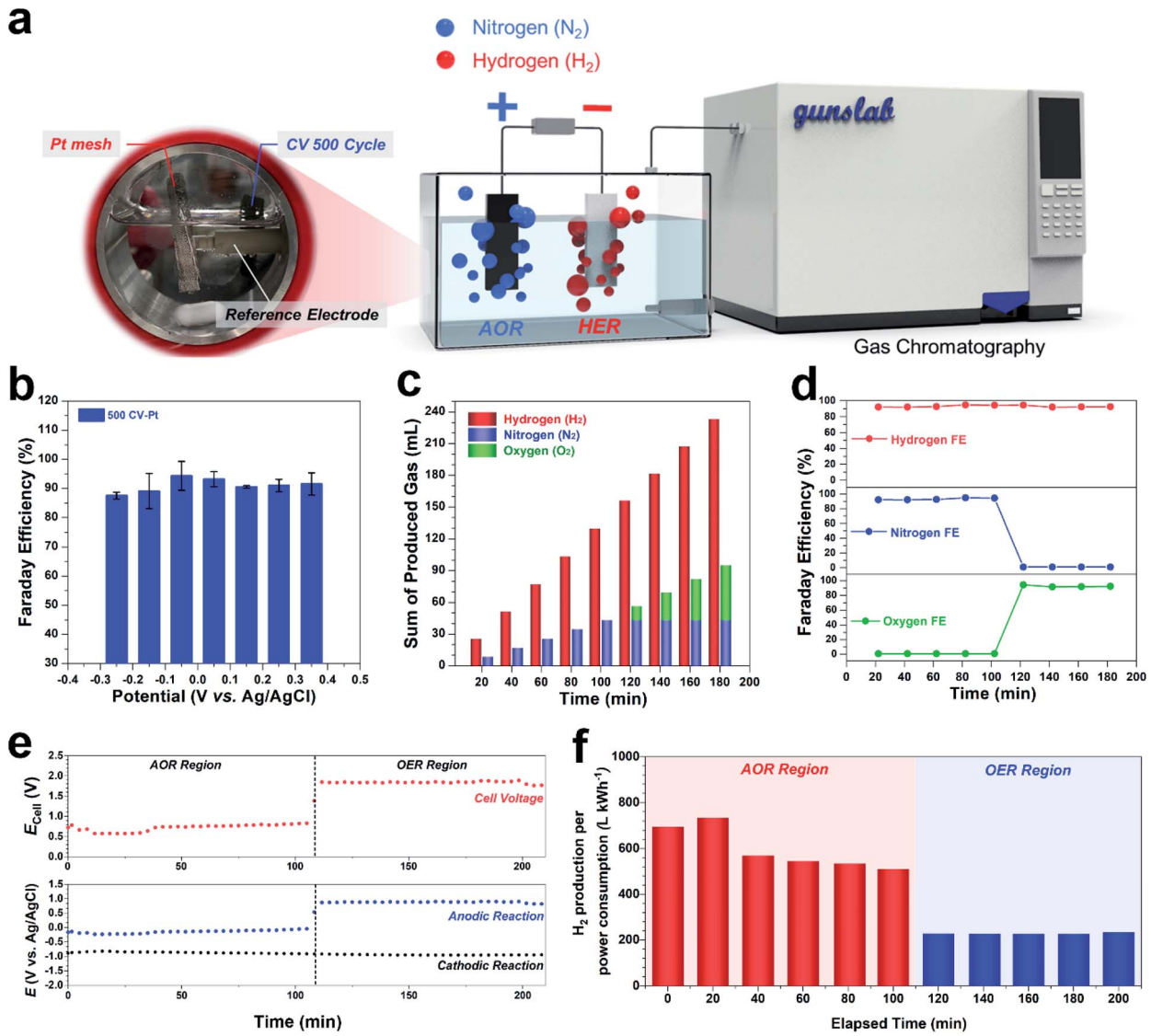

Fig. 5 (a) Schematic diagram of the *in operando* GC measurement using a three-electrode system. (b) Faradaic efficiency at a specific voltage (−0.25, −0.15, −0.05, 0.05, 0.15, 0.25, or 0.35 V). The error bar reflects the results of three devices. All electrolysis in this system was performed in 1 M NH_3 in 5 M KOH solution at 60 °C. (c) The amount (mL) and (d) faradaic efficiency (%) of each produced gas for operating ammonia electrolysis time over 200 min during discharge at 200 mA. (e) Chronopotentiometric profile in the three-electrode configuration system and (f) hydrogen production per power consumption during consecutive discharge at 200 mA.

detected at an average of *ca.* 90%, suggesting efficient AOR activities of the 500 CV-Pt electrode. Meanwhile, a separated drainage tube was utilized to determine the amount of H_2/N_2, which indicates that the gas volume and molar ratios are close to 3 : 1 between H_2 and N_2 gases (Fig. S7†) at a cell potential of 0.8 V. To investigate the AOR catalytic activity under consecutive conditions, chronopotentiometry measurements with *in operando* GC analysis were conducted at a constant current of 200 mA (Fig. 5c–f). A constant current was applied over 200 min and the amount of each gas generated was analyzed every 20 min using GC analysis. During the electrolysis process, the hydrogen and nitrogen gases were simultaneously produced with an average Faraday efficiency of 93% up to 100 min. After the anodic reaction changed from the AOR to the OER, hydrogen and oxygen gases were produced instead of nitrogen gas (Fig. 5c and d). It is worth noting that the AOR and OER processes were clearly distinguished in the case of the Pt based catalyst, but the working potential of the AOR for non-noble metal catalysts normally overlaps with the OER potential window. Therefore, it is necessary to distinguish the AOR from the OER through *in operando* analysis under practical operating conditions. At the same time, the overpotential for the anodic reaction was sharply increased from −0.05 V to 0.87 V *vs.* Ag/AgCl. The changed anodic reaction leads to significantly increased energy consumption for hydrogen production as shown in Fig. 5f. At the AOR region, the hydrogen production per power consumption was about 152% higher (568.97 L_{H2} kW h_{AOR}^{-1}) than that at the OER region (225.61 L_{H2} kW h_{OER}^{-1}).[32] These results indicate that the liquid ammonia decomposition using the 500 CV-Pt electrode has strong potential for mass

production of hydrogen at low-energy consumption in practical application.

Conclusion

In this study, we investigated electrodeposited Pt catalysts with various number of CV cycles and conducted ammonia electrolysis using a practical cell. It is noteworthy that fundamental relationships between electrodeposition cycles and electrocatalytic activity were established for the CV-Pt electrode from surface morphology analysis and electrochemical area. The enhanced catalytic activity of flower-like Pt particles in the 500 CV-Pt electrode results in stable dehydration of NH_3(aq) (0.65 V @ 50 mA cm^{-2}) as well as ammonia oxidation peak current. Moreover, the analyses discussed in the present work show that the introduction of *in operando* techniques has significantly affected the AOR study. The complex mechanisms of the AOR, which proceeds through the continuous decomposition of NH_3(aq) into NH_2 and NH species and dimerization into N_2, are distinguished from the OER competitive reaction by the simultaneous recording of the electrocatalytic performance and quantitative gas production in real time. We confirmed that highly pure hydrogen is produced with high faradaic efficiency (over 90%) and more than 60% less energy consumption (1.76 W h $L_{H_2 \text{ with AOR}}{}^{-1}$) is needed compared to conventional water electrolysis (4.43 W h $L_{H_2 \text{ with OER}}{}^{-1}$). Thus, electrocatalysts need to be developed using established experimental parameters and operating protocols for the successful implementation of NH_3(aq) as an eco-friendly energy source.

Experimental section

Electrochemical Pt deposition

The synthesis process was carried out with a three-electrode system using a Biologic VMP3. The working electrode was Ni foam (1.6 mm thickness, 99.99%, MTI Korea). A carbon rod and Ag/AgCl served as the counter and reference electrodes, respectively. In addition, the electrodeposition of Pt on Ni foam (1 cm^2) was performed under various cycle conditions with a voltage range from −0.4 to +0.2 V (*vs.* Ag/AgCl) in 0.1 M $HClO_4$ containing H_2PtCl_6 (2 mM, Sigma-Aldrich). After that, both electrodes were dried in a vacuum oven. The optimum electrodeposition conditions were determined using CVs of electrodeposited Pt at various voltages. CP electrodeposition of Pt on nickel foam was performed at a constant current of −2 mA in 0.1 M $HClO_4$ containing 2 mM H_2PtCl_6 (Sigma-Aldrich). The electrodeposited Pt electrodes were characterized using SEM (Nova Nano SEM, FEI) and XRD (D8 Advance, Bruker).

Electrochemical measurements

The experiments for ammonia electrolysis were conducted using a Biologic VMP3. A carbon rod and Ag/AgCl electrode (filled with saturated KCl) were used as the counter electrode and the reference electrode to evaluate the electrocatalytic AOR activities. To investigate the effect of pH on ammonia oxidation, CVs were recorded in 1 M NH_3(aq) electrolyte containing various concentrations of KOH ranging from 1 M to 5 M. In addition to the effect of pH, the effect of ammonia concentration was investigated by recording CVs in 5 M KOH containing concentrations of ammonia ranging from 0.1 M to 2 M NH_3(aq). CVs were carried out at a scan rate of 20 mV s^{-1} in the region from −0.40 to 0.60 V (*vs.* Ag/AgCl). Furthermore, stability profiles were investigated at various constant current densities ranging from 50 to 100 mA cm^{-2}. The obtained gas mixture was then directly subjected to analysis using a GC.

Gas chromatography analysis

The practical ammonia electrolysis system is composed of an AOR electrode (anode), HER electrode (cathode), and reference electrode (Ag/AgCl) in a three electrode system. The gas generated during operation was analyzed using a gas chromatograph with a thermal conductivity detector (GC-TCD, controlled at 290 °C) utilizing argon gas as the carrier gas (GC-2010 Plus, SHIMADZU Co.). The used column (controlled at 150 °C) is a micropacked column (ShinCarbon ST 100/120 2 m, 1 mm ID, 1/16 in OD). In addition, a 1 mL sample loop (=sample volume) for GC analysis was used. Before the *in operando* analysis, cleaning of the nitrogen (N_2) and oxygen (O_2) residue in the system is very important, because the N_2 & O_2 residue may contain substantial impurities in the Faraday profiles of each gas. We have tested the residual quantity of each gas by first saturating our solution of 5 M KOH + 1 M NH_3(aq) (40 mL of electrolyte used) with Ar to remove any excess N_2 and O_2, followed by flowing 50 sccm for 1 h. A water trap was placed before the GC instrument. After the Ar saturation process, all ammonia analysis for FE was estimated with flowing 25 sccm Ar carrier gas. Although ammonia (NH_3) in the solution could be volatile, we have also checked the absence of O_2 and N_2 peaks without any impurity after the Ar saturation process. Each standard gas was composed of Ar gas, and was quantified from the integrated peak area. Although the electrolysis was performed under consecutive conditions, the GC analyzes by a dose but not in consecutive real-time. For the sum of each produced gas, when the consecutive gas was flowed into the GC and out, 1 mL (=volume of sample loop) of sample in flowing gas was analyzed every 20 min. From the FE results of each gas, we have calculated the amount of gas produced assuming that the system was operated with identical FE between every 20 minutes.

Author contributions

Y. Y., J. K., and G. K. conceived the designed research. Y. Y. and J. K. performed the electrochemical analysis and discussed the idea for the system. A. S., and H. J. performed surface structure analysis. M. Z., H. K., and M. G. discussed the results and analyzed the data. Y. H. provided thoughtful comments. The work was conceived and supervised by G. K. All authors contributed to writing the manuscript.

Conflicts of interest

The authors declare no competing financial interests.

Acknowledgements

This work was supported by the Mid-Career Researcher Program (NRF-2018R1A2A1A05077532) through the National Research Foundation Korea, funded by the Ministry of Science, ICT, and Future Planning. Partial support from the "CO_2 utilization battery for hydrogen production based on fault-tolerance deep learning" (1.200097.01) is also acknowledged. This research was also supported by Lotte Chemical Corporation (2.190272.01).

References

1 M. Cooper and G. G. Botte, *J. Electrochem. Soc.*, 2006, **153**, A1894.
2 J. Gwak, M. Choun and J. Lee, *ChemSusChem*, 2016, **9**, 403–408.
3 F. Vitse, M. Cooper and G. G. Botte, *J. Power Sources*, 2005, **142**, 18–26.
4 D. J. Little, M. R. Smith and T. W. Hamann, *Energy Environ. Sci.*, 2015, **8**, 2775–2781.
5 J. Gwak, M. Choun and J. Lee, *ChemSusChem*, 2016, **9**, 403–408.
6 J. Huang, J. Cai and J. Wang, *ACS Appl. Energy Mater.*, 2020, **3**, 4108–4113.
7 Y. Zhou, G. Zhang, M. Yu, X. Wang, J. Lv and F. Yang, *ACS Sustain. Chem. Eng.*, 2018, **6**, 8437–8446.
8 H. Dotan, A. Landman, S. W. Sheehan, K. D. Malviya, G. E. Shter, D. A. Grave, Z. Arzi, N. Yehudai, M. Halabi, N. Gal, N. Hadari, C. Cohen, A. Rothschild and G. S. Grader, *Nat. Energy*, 2019, **4**, 786–795.
9 K. Jiang, B. Liu, M. Luo, S. Ning, M. Peng, Y. Zhao, Y. R. Lu, T. S. Chan, F. M. F. de Groot and Y. Tan, *Nat. Commun.*, 2019, **10**, 1–9.
10 J. Wu and H. Yang, *Acc. Chem. Res.*, 2013, **46**, 1848–1857.
11 B. P. Vinayan and S. Ramaprabhu, *Nanoscale*, 2013, **5**, 5109.
12 N. Cheng, S. Stambula, D. Wang, M. N. Banis, J. Liu, A. Riese, B. Xiao, R. Li, T.-K. Sham, L.-M. Liu, G. A. Botton and X. Sun, *Nat. Commun.*, 2016, **7**, 13638.
13 J. Kim, C. Kim, I. Y. Jeon, J. B. Baek, Y. W. Ju and G. Kim, *ChemElectroChem*, 2018, 1–7.
14 J. Mahmood, F. Li, S.-M. Jung, M. S. Okyay, I. Ahmad, S.-J. Kim, N. Park, H. Y. Jeong and J.-B. Baek, *Nat. Nanotechnol.*, 2017, **12**, 441–446.
15 J. Kim, Y. Yang, A. Seong, H. J. Noh, C. Kim, S. Joo, A. Cho, L. Zhang, J. Zhou, J. Q. Wang, J. W. Han, J. Mahmood, J. B. Baek and G. Kim, *J. Mater. Chem. A*, 2020, **8**, 14927–14934.
16 Y. Yang, J. Kim, C. Kim, A. Seong, O. Kwon, J. H. Lee, I. Kristanto, L. Zhang, J. Zhou, J. Q. Wang, J. B. Baek, S. K. Kwak and G. Kim, *Nano Energy*, 2020, **76**, 105114.
17 J. N. Tiwari, S. Sultan, C. W. Myung, T. Yoon, N. Li, M. Ha, A. M. Harzandi, H. J. Park, D. Y. Kim, S. S. Chandrasekaran, W. G. Lee, V. Vij, H. Kang, T. J. Shin, H. S. Shin, G. Lee, Z. Lee and K. S. Kim, *Nat. Energy*, 2018, **3**, 773–782.
18 G. Jerkiewicz, G. Vatankhah, J. Lessard, M. P. Soriaga and Y. S. Park, *Electrochim. Acta*, 2004, **49**, 1451–1459.
19 B. E. Conway, *J. Electroanal. Chem.*, 2002, **524–525**, 4–19.
20 S. Choi, S. Park, J. Shin and G. Kim, *J. Mater. Chem. A*, 2015, **3**, 6088–6095.
21 M. Palcut, R. Knibbe, K. Wiik and T. Grande, *Solid State Ionics*, 2011, **202**, 6–13.
22 S. Kim, A. Jun, O. Kwon, J. Kim, S. Yoo, H. Y. Jeong, J. Shin and G. Kim, *ChemSusChem*, 2015, **8**, 3153–3158.
23 A. K. Hill and L. Torrente-Murciano, *Int. J. Hydrogen Energy*, 2014, **39**, 7646–7654.
24 J. L. Cao, Z. L. Yan, Q. F. Deng, Y. Wang, Z. Y. Yuan, G. Sun, T. K. Jia, X. D. Wang, H. Bala and Z. Y. Zhang, *Int. J. Hydrogen Energy*, 2014, **39**, 5747–5755.
25 A. C. A. De Vooys, M. T. M. Koper, R. A. Van Santen and J. A. R. Van Veen, *J. Electroanal. Chem.*, 2001, **506**, 127–137.
26 C. Kim, J. Kim, S. Joo, Y. Yang, J. Shin, M. Liu, J. Cho and G. Kim, *Angew. Chem., Int. Ed.*, 2019, **58**, 9506–9511.
27 H. Zhang, Y. Wang, Z. Wu and D. Y. C. Leung, *Energy Procedia*, 2017, **142**, 1539–1544.
28 B. K. Boggs and G. G. Botte, *Electrochim. Acta*, 2010, **55**, 5287–5293.
29 N. M. Adli, H. Zhang, S. Mukherjee and G. Wu, *J. Electrochem. Soc.*, 2018, **165**, J3130–J3147.
30 X. Xu, Y. Chen, W. Zhou, Z. Zhu, C. Su, M. Liu and Z. Shao, *Adv. Mater.*, 2016, 6442–6448.
31 A. Seong, J. Kim, O. Kwon, H. Y. Jeong, R. J. Gorte, J. M. Vohs and G. Kim, *Nano Energy*, 2020, **71**, 104564.
32 D. H. Kweon, M. S. Okyay, S. J. Kim, J. P. Jeon, H. J. Noh, N. Park, J. Mahmood and J. B. Baek, *Nat. Commun.*, 2020, **11**, 1–10.